Climate Dynamics (1996) 12:381–388

Climate Dynamics

A global ocean mesh to overcome the North Pole singularity

Gurvan Madec, Maurice Imbard

Laboratoire d'Océanographie Dynamique et de Climatologie (CNRS/ORSTOM/UPMC), Université Paris VI, boîte 100, 4, place Jussieu, 75252 Paris, France

Received: 21 June 1995 / Accepted: 9 November 1995

Abstract. A semi-analytical method is presented for constructing a global orthogonal curvilinear ocean mesh which has no singularity point inside the computational domain since the mesh poles are moved to land points. The method involves defining an analytical set of mesh parallels in the stereographic polar plan, computing the associated set of mesh meridians, and projecting the resulting mesh onto the sphere. The set of mesh parallels proposed here is defined as a series of embedded circles. The resulting mesh presents no loss of continuity in either the mesh lines or the scale factors over the whole ocean domain, as the mesh is not a composite mesh. Thus, the Bering Strait can be opened without specific treatment. The equator is a mesh line, which provides a better numerical solution for equatorial dynamics. The resolution can be easily controlled through the definition of three analytical functions which can increase resolution and/or maintain a low ratio of anisotropy. The mesh has been implemented in the LODYC general circulation ocean model. Results of a semi-diagnostic simulation are shown.

1 Introduction

The Arctic Ocean is an active participant in the global climate system which influences both its oceanic and atmospheric components. The sea ice export and fresh polar surface water outflow regulate the deep convection in the Nordic Seas (Aagaard and Carmack 1989), while the deep Arctic water outflow actively contributes to the formation of the North Sea deep water. All these exchanges ultimately determine the characteristics of the North Atlantic Deep Water and have a significant impact on the global ocean "conveyor belt". Due to the presence of a permanent sea ice cover involving strong positive feedbacks between the atmosphere and the ocean (Herman and Johnson 1980), the Arctic Ocean is also suspected to play a central role in the natural variability of the climate system (Mysak et al. 1990). Model experiments have also shown that it is quite vulnerable to large climatic changes from increased atmospheric CO_2 as a result of positive feedbacks related to high latitude snow and sea ice (Washington and Meehl 1986).

The Arctic Ocean stratification plays a crucial role in maintaining the sea ice cover as well as in controlling the efficiency of the deep water formation on the shelves. The stratification is itself controlled by the surface fresh water input from river run-off and through the Bering Strait, and by the warm, salty inflow of Atlantic water from the Nordic Seas (Rudels 1989). In particular, the influence of the Bering Strait inflow on the global ocean circulation has recently been emphasized by Reason and Power (1994) in a numerical study. They show an increase of 8% in the rate of formation of the North Atlantic Deep Water when the strait is open.

In the development of a global ocean model for climate purposes as well as for the study of the global thermohaline circulation, it is therefore important to include the Arctic Ocean and its connections to the Atlantic and Pacific Oceans. Unfortunately, the traditional geographical latitude-longitude coordinate system used in solving the equations of motion in ocean general circulation models has a singular point in the Arctic Ocean at the North Pole, where the meridians converge inside the computational domain. The convergence places a severe restriction on the length of the time step allowed for computational stability of finite difference schemes. Various solutions have been advanced to solve this problem. Bryan et al. (1975) applied a zonal Fourier filter poleward of 45° on the prognostic fields in order to suppress the shortest wavelength components. However, this procedure can generate numerical noise as the non divergent nature of the flow is not necessarily preserved by the filter (Bryan 1987). Semtner and Chervin (1988) suppress the problem by the walling off of the Arctic Ocean at

Correspondence to: G. Madec

65°N latitude. Another solution consists of using a composite mesh made up of two grids rotated by 90° relative to each other (one mesh's poles are on the other grid's equator) (Deleersnijder et al. 1993; Eby and Holloway 1994; Gwilliam 1995). One mesh is used for the North Atlantic and Arctic Oceans and the other for the rest of the world ocean. The Bering Strait is closed and the two meshes are coupled along a line of longitude in one mesh and along the equator in the other. Although this solution solves the North Pole problem, it still presents two drawbacks. First, the grid size cannot be continuous across the equator: a small change in grid size occurs across the equator which can damage the second order accuracy of the numerical schemes used in the ocean model (Marti et al. 1992). However, the effect of such a discontinuity may be small as suggested by Coward et al. (1994). Second, the mesh does not link the Pacific Ocean to the Arctic Ocean continuously, so that a specific treatment must be developed to open the Bering Strait.

The solution proposed in this study overcomes the North Pole singularity without these drawbacks, but requires an ocean model adapted to horizontal orthogonal curvilinear coordinates. It consists of covering the Earth with a global orthogonal curvilinear mesh in which the poles (i.e. points of convergence of mesh line) are located on land. Various methods exist for constructing such a mesh. Murray (1995) shows that a number of global orthogonal curvilinear meshes can be constructed quite simply by analytical means, using the properties of conformal map projection. However, the equatorial dynamics is better solved numerically when the mesh parallels have an east-west alignment at the equator. This additional requirement makes it necessary to resort to the use of composite meshes, when using analytical meshes proposed by Murray (1995). This inevitably results in some loss of continuity of scale factors (metric coefficients) across the join (Murray 1995). The method proposed here is a semi-analytical method which allows global orthogonal curvilinear meshes to be constructed for which poles are on land and the equator is a mesh line.

The study is structured as follows: in Sect. 2 the technique used to defined the global ocean mesh is described. In Sect. 3, the choice of the various parameters is discussed. In the last section the results obtained for a global ocean model are briefly presented.

2 Construction of the horizontal global mesh

The basic idea of the mesh construction is to define judiciously an analytical set of mesh parallels. A differential equation can be derived that must be verified by the mesh meridians. The numerical solution of this equation completes the global mesh construction. In order to simplify both the definition of the mesh parallels and the resolution, it is convenient to work on a north stereographic polar plan rather than on a sphere. Indeed, since the stereographic polar projection is a conformal transformation, the projection on the sphere of an orthogonal mesh defined on this plan is also an orthogonal mesh. The problem can thus be reduced to a two-dimensional problem of defining an analytical set of mesh parallels and computing the corresponding mesh meridians on the stereographic polar plan.

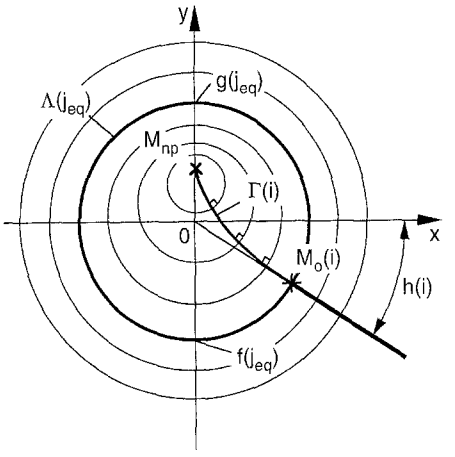

Fig. 1. In the stereographic polar plan (Ox, Oy), the mesh parallels $\Lambda(j)$ are a series of embedded circles which have the same centre O outside $\Lambda(j_{eq})$ and which have centres that continuously move along the y-axis from O to M_{np} inside $\Lambda(j_{eq})$. Starting from point $M_0(i)$ defined by the angle $h(i)$, a mesh meridian $\Gamma(i)$ is computed as the curve which intercepts each circle $\Lambda(j)$ at right angles

Let the horizontal ocean mesh be defined by the I- and J-curves, the mesh meridians and parallels, respectively. IM and JM are the number of I- and J-curves covering the global mesh, and J_{eq} is the number of J-curves in the Southern Hemisphere. Let (Ox, Oy) be a Cartesian coordinate system on the north stereographic polar plan such that O and the unity circle are the stereographic polar projection of the North Pole and the equator, respectively (Fig. 1).

2.1 *The choice of J-curves*

The J-curves are defined as a series of embedded circles which have the same centre O in the Southern Hemisphere (i.e. outside the unity circle) and which have centres that continuously move along the y-axis from O to M_{np} (the mesh North Pole) in the Northern Hemisphere (i.e. inside the unity circle) (Fig. 1). This series of circles $\Lambda(j)$ is defined for both hemispheres by the following equation:

$$\Lambda(j): x^2+y^2-(f(j)+g(j))y+f(j)g(j)=0 \quad j\in[1,JM] \quad (1)$$

where f and g are the functions which give the ordinate of the two intersections between $\Lambda(j)$ and the y-axis. f and g verify the following properties:

f and g are continuous and differentiable at least twice (a)

f is strictly increasing and g is strictly decreasing with increasing j (b)

$f(JM)=g(JM)$ (c)

$$f(J_{eq}) = -1 = -g(J_{eq}) \quad \text{(d)}$$

$$f(j) = -g(j) \quad j \in [1, J_{eq}] \quad \text{(e)}$$

Conditions (a) and (b) ensure that the circles are strictly embedded and that given a point $M=(x,y)$ on the stereographic plan, there exists one and only one $j \in [1, JM]$ which verifies (1); (c) that $\Lambda(JM)$ reduces to a single point, the mesh North Pole M_{np}; (d) that $\Lambda(J_{eq})$ is the unity circle, so that the equator is a mesh line; and (e) that outside the unity circle, all the circles are centred on O (i.e. the Southern Hemisphere configuration is geographical). Note that (e) can be modified to shift the mesh South Pole. This is a priori not necessary as the South Pole is already placed near the centre of the Antarctic continent.

2.2 *Computation of the I-curves*

The I-curves form a series of curves $I(i)$ which cross the equatorial circle $\Lambda(J_{eq})$ at a point $M_0(i)$ defined by the angle $(Ox, OM_0) = h(i)$, where h is a given continuous and at least twice differentiable function (Fig. 1). h describes the I-point distribution along the equator. The I-curves intercept each circle $\Lambda(j)$ at right angles, i.e. they obey the following differential equation:

$$\frac{dy}{dx} = \frac{2y - (f(j) + g(j))}{2x} \tag{2}$$

Since j is linked to (x,y) through Eq. (1), an analytical solution for Eq. (2) is by no means trivial except for particular expressions of f and g which do not verify all the properties (a) to (e). For example, when f and g are linear functions of j, the curves $I(i)$ which are solutions of Eq. (2) also form a linear series of embedded circles but the resulting mesh does not have a latitude/longitude configuration in the Southern Hemisphere. However, Eq. (2) can be solved numerically with a very high precision to find the I-curves. The algorithm used to compute the pairs $(x(i,j), y(i,j))$ is presented in the appendix. The geographical coordinates of all the mesh points on the sphere are then obtained by applying the inverse of the stereographic polar projection:

$$\begin{aligned} \lambda(i,j) &= \frac{180^\circ}{\pi} \arctan\left(\frac{y(i,j)}{x(i,j)}\right) \\ \varphi(i,j) &= 90^\circ - \frac{360^\circ}{\pi} \arctan\left(\sqrt{x^2(i,j) + y^2(i,j)}\right) \end{aligned} \tag{3}$$

In order to complete the mesh computation, we have to evaluate the scale factors (i.e. the rate of deformation of the mesh or grid spacing) in the two horizontal directions. These scale factors e_1 and e_2 are given by:

$$\begin{aligned} e_1 &= a\left[\left(\frac{\partial \lambda}{\partial i}\cos\varphi\right)^2 + \left(\frac{\partial \varphi}{\partial i}\right)^2\right]^{1/2} \\ e_2 &= a\left[\left(\frac{\partial \lambda}{\partial j}\cos\varphi\right)^2 + \left(\frac{\partial \varphi}{\partial j}\right)^2\right]^{1/2} \end{aligned} \tag{4}$$

where a is the Earth's radius. The partial derivative of λ and φ with respect to i and j are computed using a fourth order centred finite difference scheme. A sufficient precision is reached for this computation by using a mesh which is one hundred times smaller than the mesh required. We verify the overall precision of the above mesh computation in the case of linear f and g functions where an analytical solution is known, and in the general case, by computing a mesh that was one thousand times smaller than the required one. In both cases, the accuracy of the mesh point positions and of the scale factors was found to be smaller than 10^{-5} m, that is a relative precision smaller than 10^{-10}.

3 Choice of a global ocean mesh

The technique presented in the previous section allows the definition of various global ocean meshes, depending on the mesh North Pole position (M_{np}) and the functions f, g and h chosen. The expected resolution will serve as guideline between the different choices. Here, we want to define a world ocean model to study the seasonal to decadal variability of the ocean with special attention devoted to the tropical interannual variability. The model resolution must be a reasonable compromise between ocean physics and computational resources. This leads, for the Southern Hemiphere, to a zonal grid spacing of 2°, and to a meridional grid spacing of 1.5° at mid-latitudes decreasing to 0.5° in the equatorial strip. For the Northern Hemisphere, the mesh characteristics must be similar, in particular the scale factors must not be smaller than in the Southern Hemisphere, otherwise it would result in a more restrictive CFL criterion. Therefore, the mesh North Pole has been set at 40°N and 90°E, i.e. over China. This is as far as possible from the geographical North Pole while being not too close to an oceanic area. The choice of h is straightforward and corresponds to a uniform 2° grid spacing along the equator:

$$h(i) = 2i \quad 1 \le i \le IM \tag{5}$$

where h is expressed in degrees and $IM = 180$.

For f and g, the analytical expression is somewhat more complicated. We found it convenient to define f' and g', the first derivative of f and g, as linear combinations of hyperbolic tangents plus a constant (Fig. 2), so that the grid spacing can be rather easily adjusted to the desired values. f and g expressed in degrees, take the following form:

$$\begin{aligned} f(j) &= A_0 j + A_1 \\ &+ B_0 \log[\cosh[(j - J_{eq} - J_B)/B_1]/\cosh[(j - J_{eq} + J_B)/B_1]] \\ &- C_0 \log[\cosh[(j - J_{eq} - J_C)/C_1]/\cosh[(j - J_{eq} + J_C)/C_1]] \end{aligned} \tag{6a}$$

$$\begin{aligned} &\text{for } 1 \le j \le J_{eq} \quad g(j) = f(j) \\ &\text{for } J_{eq} \le j \le JM \quad g(j) = D_0 j + D_1 \\ &- E_0 \log[\cosh[(j - J_{eq} - J_E)/E_1]/\cosh[(j - J_{eq} + J_E)/E_1]] \end{aligned} \tag{6b}$$

The first (second) logarithmic term of Eq. (6a) is responsible for a symmetrie change with respect to the

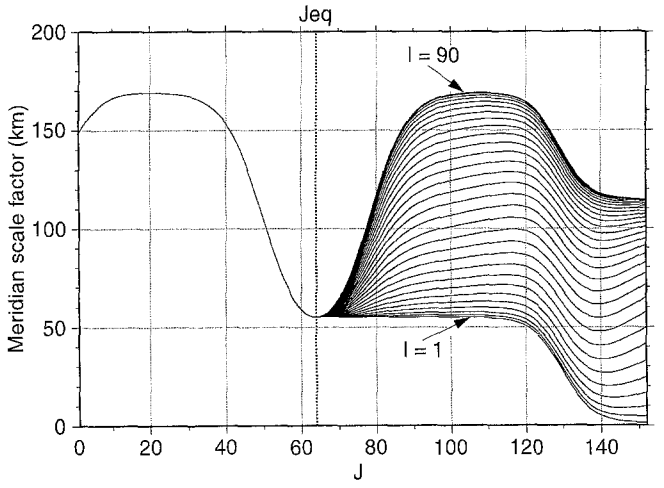

Fig. 2. Meridian scale factor e_2 as a function of the mesh parallel index J. Each curve is associated with an integer value of the mesh meridian index I. The envelope of these curves ($I=1$ and $I=90$) gives the first derivative of g and f

equator in the grid spacing between the equator and mid-latitudes (mid-latitudes and polar regions) (Fig. 2). The logarithmic term of Eq. (6b) is responsible for the decrease of the grid spacing northward of 30°N, over Asia (Fig. 2) which allows the grid pole to be at 40°N. The choice of the 15 coefficients in Eqs. (6a) and (6b) is as follows. We first set the number of grid points in the north-south direction and the index of the equator: $JM=150$ and $J_{eq}=64$. Then, we choose $B_1=10.$, $J_B=14$ and $B_0=0.52\ B_1/\tanh[J_B/B_1]$ which means that the variation of f' from its equatorial value to its mid-latitude value occurs over 10 points at the 14th point on both sides of the equator point, and with an amplitude of $2\times0.52=1.04°$. Similarly, we choose $C_1=8.$, $J_C=65$ and $C_0=0.25\ C_1/\tanh[J_C/C_1]$ for the variation of f' over polar regions. A_0 and A_1 are then specified such that $f'(J_{eq})=0.5°$ and $f(J_{eq})=0°$, which leads to $A_0=0.5+2\times0.52-2\times0.25=1.04°$ and $A_1=-A_0J_{eq}$.

A similar procedure is used for g. We set $E_1=8.$ and $J_E=65$ and choose E_0 such that g' varies from 0.5° at the equator to a minimum value of 10^{-2} at $j=JM$. This last condition ensures that g' is strictly positive ($g'>0$), i.e. the property (a) is satisfied. It leads to the following expression for E_0:

$$E_0=(0.5-10^{-2})/E_1/(2\tanh[J_E/E_1]-\tanh[(JM-J_{eq}-J_E)/E_1]+\tanh[(JM-J_{eq}+J_E)/E_1])$$

The value of D_0 and D_1 are then specified such that $g'(J_{eq})=0.5°$ and $g(J_{eq})=0°$, which leads to $D_0=0.5-2E_0\tanh(J_E/E_1)/E_1$ and $D_1=-D_0J_{eq}$.

Using these coefficients, f and g satisfy (a) to (e), apart from (c). For this last property, they can always be extended toward the mesh North Pole while verifying the other required properties. However this part of the mesh is on a continent, i.e. out of the computational domain, so that it is not required.

Using the above functions and mesh North Pole position and the numerical procedure described in the previous paragraph, a global ocean mesh has been computed. Its ocean/land masked stereographic north polar projection is shown in Fig. 3. The associated masked scale factors and ratio of anisotropy, $R_i=\max(e_1/e_2,e_2/e_1)$, are shown in Fig. 4. The mesh has 180×150 grid points. The minimum value of the scale factors, 50 km, is reached in the Kara and Weddell Seas. The ratio of anisotropy is maximum at the equa-

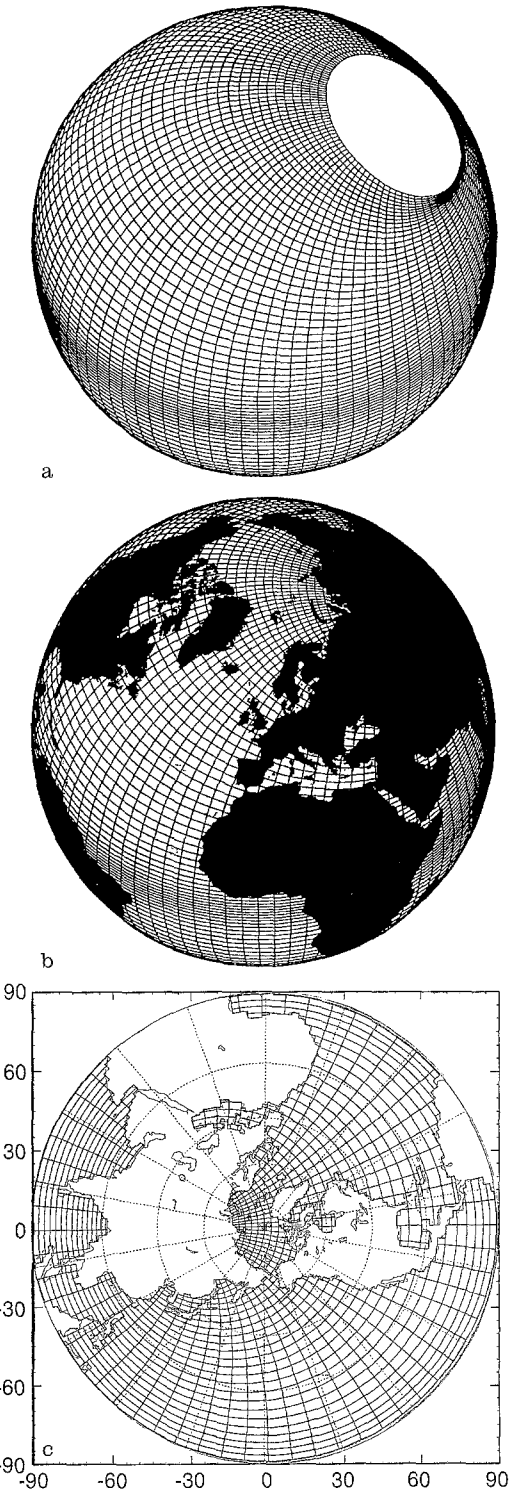

Fig. 3. a Unmasked and **b** masked world ocean mesh and **c** stereographic north polar projection of the world ocean mesh. Only one mesh parallel and meridian in three are shown

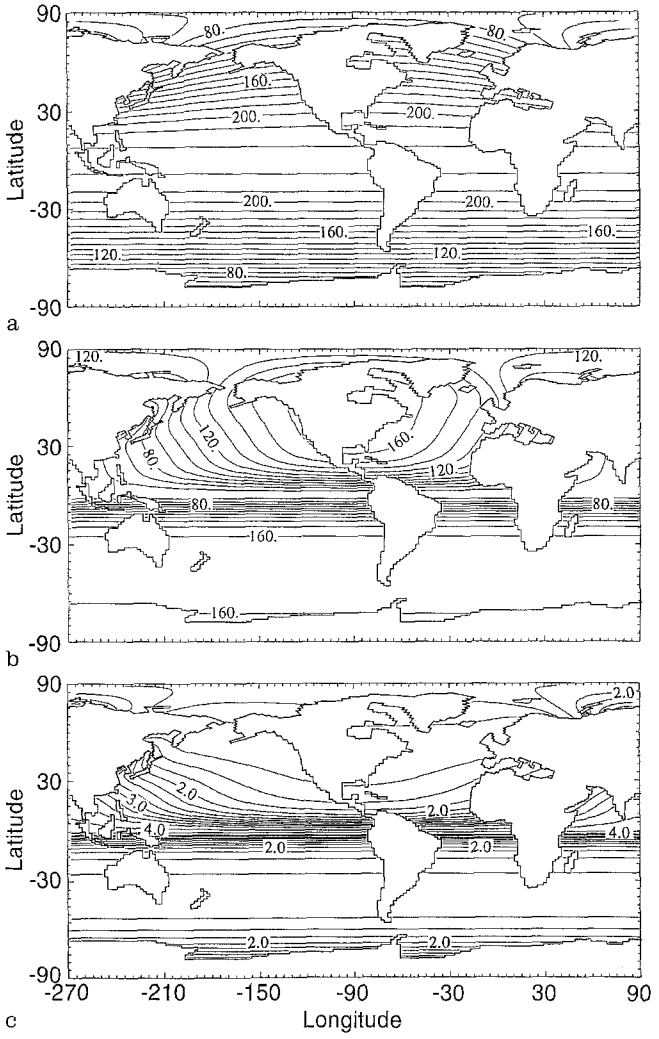

Fig. 4. **a** Horizontal scale factors e_1 and **b** e_2 of the world ocean mesh and **c** the associated ratio of anisotropy, $R_i = \max(e_1/e_2, e_2/e_1)$. The contour interval is 10 km in **a** and **b**, and 0.25 in **c**

tor where it is equal to 4 ($2° \times 0.5°$). It slowly decreases to 1 at mid-latitudes and then increases poleward to 3 at the end of the Kara and Weddell Seas. This ratio remains below its equatorial value because of the decrease of f' in polar regions.

4 Results of the global ocean model

The mesh described in the previous section has been used in the Laboratoire d'Océanographie Dynamique et de Climatologie (LODYC) primitive equation ocean general cirulation model (Delecluse et al. 1993) to simulate the global ocean circulation associated with the thermodynamic fields of Levitus (1982). The limiting factor for the time step is not the smallness of the scale factors, but the value reached by the Coriolis parameter at the North Pole. Indeed, the time step must verify $2\pi f \Delta t \leq 1$ which leads to a maximum time step of 1 h 55 min. As the time discretization of the Coriolis term is explicit in the model, this is the most restrictive constraint on the time step which has led us to choose a model time step of 1 h 40 min.

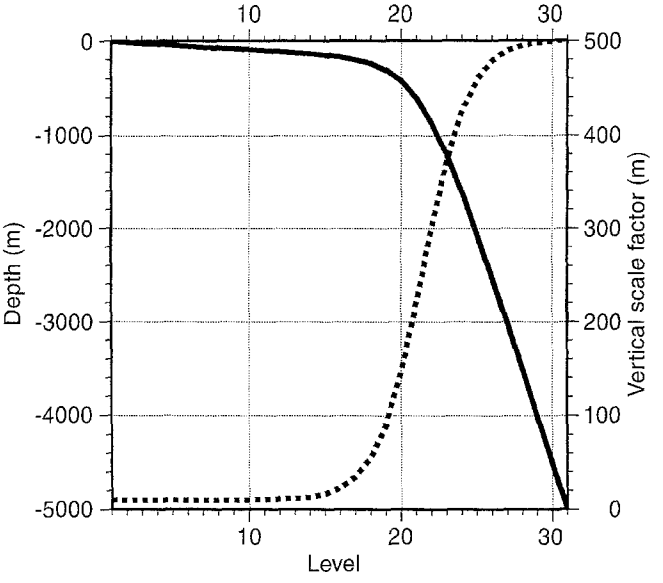

Fig. 5. Model level depth(*thick line*) and associated vertical scale factors (*dashed line*)

In the vertical, the placement of vertical velocity and temperature levels is defined from an analytic expression of the depth $z(k)$ whose derivative provides the vertical scale factor $e_3(k) = \partial z/\partial k$ (Marti et al. 1992). The following function has been chosen:

$$z(k) = h_0 - h_1 k - h_2 h_3 \log\left[\cosh\left(\frac{k - h_4}{h_3}\right)\right] \tag{7}$$

where $k = 1$ to KM for vertical velocity levels and $k = 1 + 1/2$ to $KM + 1/2$ for temperature levels. Such an expression allows us to define a nearly uniform placement of levels at the ocean top and bottom with a smooth hyperbolic tangent transition in between (Fig. 5). Here we have chosen a 10 m (500 m) resolution in the surface (bottom) layers and a depth which varies from 0 at the sea surface to a minimum of -5000 m. This leads to the following conditions:

$$\begin{aligned} &e_3(1 + 1/2) = 10. \\ &e_3(KM - 1/2) = 500. \\ &z = 0. \\ &z(KM) = -5000. \end{aligned} \tag{8}$$

The five coefficients h_0 to h_4 in Eq. (7) are determined such that Eq. (8) is satisfied. To do so, we first made an arbitrary choice of KM and h_3, here $KM = 31$ and $h_3 = 3$. Using the first three conditions in Eq. (8), we express h_0 h_1 and h_2 as a function of h_4, and then we determine $h_4 \in [1, KM]$ using a bisection method such that the last condition in Eq. (8) is satisfied. In the present case this leads to the following values: $h_0 = 4762.96$, $h_1 = 255.58$, $h_2 = 245.58$, and $h_4 = 21.43$. The resulting depths and scale factors as a function of the model levels are shown in Fig. 5.

The global model has eleven islands: Antarctica, America, Cuba, Madagascar, Philippines, Borneo, New

Guinea, Australia, New Zealand, Iceland and Spitzbergen. Non-zero depth-integrated circulation is permitted around each island. The bottom topography field is derived from the 5′ × 5′ ETOPO5 (1986) averaged over each model tracer grid box. A minimum depth for the ocean continental shelf has been set to 3 levels (~30 m) and a maximum depth to 5000 m. Finally, no smoothing operator has been applied on the resulting bathymetry, but alterations were made by hand to improve representation of major ridges and sills. In particular, a width of at least two tracer grid points has been imposed on straits and deep channels. This constraint is motivated by the discrete expression of the geostrophic balance which requires the definition of a pressure gradient across the straits and channels.

Horizontal eddy viscosity and diffusivity coefficients were set to $4\ 10^4\ m^2\ s^{-1}$ and $2\ 10^3\ m^2\ s^{-1}$, respectively, while the vertical ones are computed from a 1.5 turbulent closure model (Blanke and Delecluse 1993). The model was forced with monthly Hellerman and Rosenstein (1983) wind stress and Esbensen and Kushnir (1981) heat flux climatology plus a 12 day relaxation toward surface time varying temperature and salinity data of Levitus (1982). The integration was started with January Levitus (1982) data and pursued over a 20 year period with an interior relaxation to the monthly mean temperature and seasonal mean salinity of Levitus (1982) with a relaxation time scale of 50 days in the upper 800 m and 1 year in the deep ocean.

To give an exhaustive description of the simulated dynamics is beyond the scope of this study. A brief presentation of the annual mean circulation integrated either vertically or zonally is preferred to highlight the simulation behaviour. The annual mean barotropic stream function (BSF) associated with the vertically integrated horizontal circulation is shown in Fig. 6a. In middle and low latitudes and away from the western boundaries and straits, the BSF almost reflects the Sverdrup transport derived from wind stress. The magnitude of tropical and sub-tropical gyres is similar to those obtained in other global models using the same wind product (see for example Semtner and Chervin 1992). A zoom in the BSF field over the Arctic Ocean given in Fig. 6b emphasizes the importance of the flow through the Bering Strait on the Arctic circulation. Although the low model resolution in this region (~110 km, Fig. 3c) leads us to a widening of the Bering Strait from 85 to 220 km (two temperature and velocity grid points) with an adequate depth of 40 m, about 0.95 Sv ($1\ Sv = 10^{-6}\ m^3\ s^{-1}$) enters the Arctic Ocean through the Bering Strait in good agreement with observations (Coachman and Aagaard 1988). This is only three times less than the net inflow west of Iceland (3.4 Sv) and allows the Denmark Strait net outflow to be 22% higher (4.35 Sv).

Figure 7 shows the annual mean meridional stream function (MSF) associated with the zonally integrated meridional circulation both for the global circulation (Fig. 7a) and for the circulation only in the Atlantic

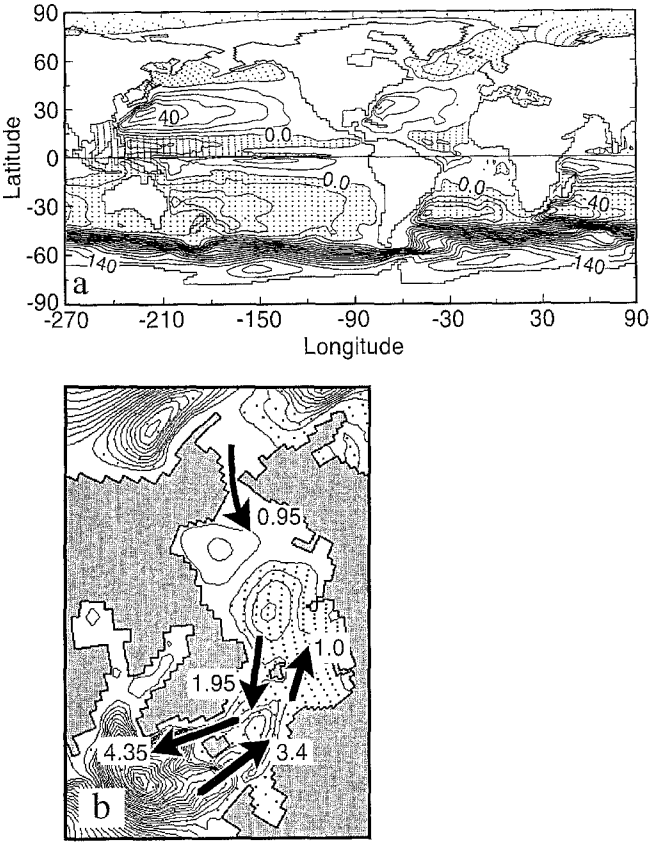

Fig. 6. a Annual mean barotropic stream function associated with the vertically integrated horizontal circulation and **b** zoom-in of the stream function over the Arctic ocean. The contour interval is 10 and 1 Sverdrup, respectively. The *numbers* indicate the mass transport in Sverdrup through the different Arctic straits

(Fig. 7b). The computation of these MSF is not straightforward as the mesh does not follow the longitudes in the Northern Hemisphere. MSF is deduced from a meridional flow which is computed for a given latitude as the flow that crosses a broken line which follows the faces of the mesh cells and is as close as possible to that latitude. The broken lines used for the North Atlantic MSF computation are shown in Fig. 8. This solution has been preferred to an interpolation of the velocity fields onto a geographic mesh before the computation. Indeed, such an interpolation introduces errors in the velocity, field which is no longer non-divergent, and thus the resulting MSF indicates a transport of water through the ocean floor or surface, depending on the direction of integration (Eby and Holloway 1994). The general features of both Atlantic and global MSF are similar to those obtained in other global models. No problem occurs that could be related to the stretched mesh used. Such a mesh appears to be well suited to the simulation of the global ocean circulation.

5 Conclusion

A semi-analytical method has been developed to construct a global orthogonal curvilinear ocean mesh. It

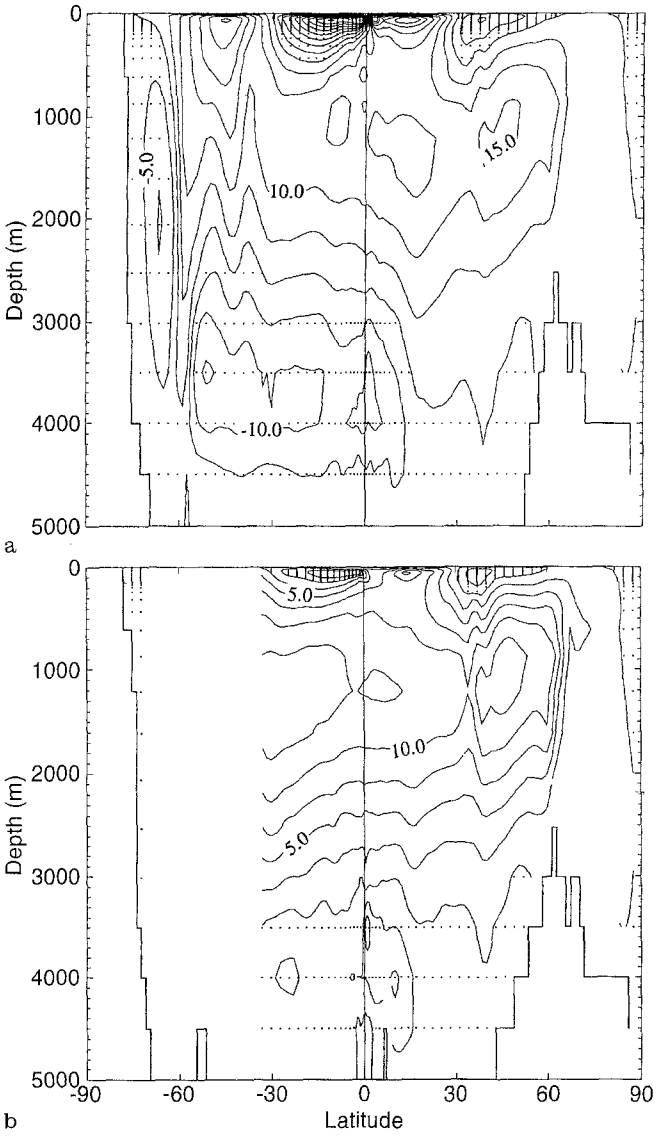

Fig. 7a, b. Annual mean meridional stream function associated with the zonally integrated meridional circulation for **a** the global circulation and **b** the circulation only in the Atlantic. The contour interval is 5 and 2.5 Sverdrup, respectively

consists in defining an analytical set of mesh parallels on a stereographic polar plan, then deriving and solving a differential equation to compute the associated set of mesh meridians, and eventually projecting the resulting mesh onto the sphere. The set of mesh parallels used here has been defined as a series of embedded circles. It provides a world ocean mesh which has the following properties: (1) the mesh has no singularity point inside the computational domain as the mesh North Pole has been shifted onto land ; (2) no loss of continuity of either the mesh lines or the scale factors occurs over the whole ocean domain, as the mesh is not a composite mesh; (3) the Bering Strait is opened without specific treatment; (4) the equator is a mesh line, which provides a better numerical solution for the equatorial dynamics; and (5) the resolution can be controlled through the definition of three analytical functions to increase resolution and/or to maintain a low

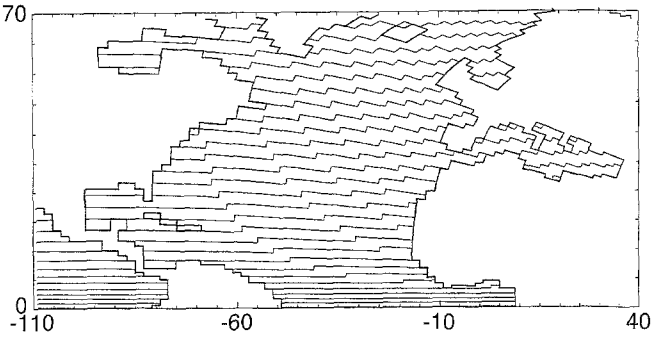

Fig. 8. The broken lines used for the North Atlantic meridional stream function computation. One line in three is shown

ratio of anisotropy (see the resolution in the equatorial and Arctic regions). A world ocean model has been designed using this technique. It gives satisfactory results and is currently being used both in forced (Madec 1995, personal communication) and coupled mode (Guilyardi et al. 1995).

The method can be applied to any other set of mesh parallels that are defined analytically, so that a differential equation can be derived and solved to find the mesh meridian. For example, a solution that exhibits similar properties to the one presented here is suggested from Murray's (1995) work. The set of mesh parallels can be defined as a series of embedded ellipses starting from the equatorial circle (or any other chosen latitude circle) and converging toward confocal ellipses whose focals are set onto North America and Russia, respectively.

Acknowledgements. Support for computation has been provided by the Institut de Recherche en Informatique Scientifique (IDRIS) of the Centre National de la Recherche Scientifique (CNRS).

Appendix: Numerical computation of *I*-curves

Outside the unity circle, the *I*-curves are half-rays, so that no computational effort is required to solve the differential Eq. (2). Inside the unity circle, Eq. (2) is solved starting from the point $M_0(i)$ using a constant grid spacing $\Delta x = \cos(h(i))/N$ (where N is the number of space steps), by the following algorithm:

– initialization:

$$(x^0, y^0) = (\cos[h(i)], \sin[h(i)])$$
$$x^1 = x^0 - \Delta x \qquad \text{(A1)}$$
$$y' = y^0 - \Delta x \left(\frac{dy}{dx}\right)^0 = y^0 - \Delta x \tan[h(i)]$$

– for $n = 1$ to N:

First, the index j^n of the circle Λ which goes through $M_n = (x^n y^n)$ is determined. This index is the solution of Eq. (1) for (y^n, y^n). The existence and uniqueness of j^n is established by (a) and (b). The index is found at the machine precision by a method of bisection. Then, y^{n+1} can be computed using a second order centred finite difference approximation of Eq. (2):

$$x^{n+1} = x^n - \Delta x$$
$$y^{n+1} = y^{n-1} + 2\Delta x \frac{2y^n - (f(j^n) + g(j^n))}{2x^n} \quad \text{(A2)}$$

Note that a higher order of approximation can be used, such as fourth order Runge-Kutta scheme, to solve Eq. (2). The choice is between increasing the accuracy of the scheme or spending an equivalent amount of extra computation time in reducing the grid spacing (larger value of N). The second alternative has been found to be more advantageous. The above computation allows each Γ-curve to be defined by a series of triplets $(x^n(i), y^n(i), j^n(i))$, then a fourth order interpolation scheme is used to find, for each integer value of i, the coordinates (x^n, y^n) associated with integer values of j. This interpolation is done with a high precision as N is typically set to one hundred times $JM - J_{eq}$.

References

Aagaard K, Carmark EC (1989) The role of sea ice and other fresh water in the Arctic circulation. J Geophys Res 94:14485–14498

Blanke B, Delecluse P (1992) Variability of the tropical Atlantic ocean simulated by a general circulation model with two different mixed layer physics. J Phys Oceanogr 23:1363–1388

Bryan F (1987) Parameter sensitivity of primitive equation ocean general circulation models. J Phys Oceanogr 17:970–985

Bryan K, Manabe S, Pacanowski RC (1975) A global ocean-atmosphere climate model. Part II. The oceanic circulation. J Phys Oceanogr 5:30–46

Coachman LK, Aagaard K (1988) Transports through Bering Strait: annual and interannual variability. J Geophys Res 93:15535–15539

Coward AC, Killworth PD, Blundell JR (1994) Tests of a two-grid world ocean model. J Geophys Res 99:22725–22735

Delecluse P, Madec G, Imbard M, Lévy C (1993) OPA version 7 Ocean General Circulation Model reference manual. LODYC, France, Internal Report, 93/05, 111 pp (Available from Laboratoire d'Océanographie Dynamique et de Climatologie, Université Paris VI, 75252 Paris, France)

Deleersnijder E, Van Ypersele JP, Campin JM (1993) An orthogonal, curvilinear coordinate system for a world ocean model. Ocean Modelling 100 (unpublished manuscript)

Eby M, Holloway G (1994) Grid transformation for incorporating the Arctic in a global ocean model. Clim Dyn 10:241–247

Esbensen SK, Kushnir Y (1981) The heat budget of the global ocean: an atlas based on estimates from marine surface observations. Climatic Resolution Institution, Oregon State, University, Rep 29

ETOPO5 (1986) Global 5′ × 5′ depth and elevation. (Available from National Geographical Data Center, NOAA, US Department of Commerce, Code E/GC3, Boulder, CO 80303)

Guilyardi E, Madec G, Terray L, Déqué M, Pontaud M, Imbard M, Stephenson D, Filiberti MA, Cariolle D, Delecluse P, Thual O (1995) Simulation couplée océan-atmosphère de la variabilité du climat. C R Acad Sci Paris, 320, Série IIa, 683–690

Gwilliam CS (1995) The OCCAM Global Ocean Model. In: Hoffman G-R, Krietz N (eds) Coming of Age (Proc 6th ECMWF Workshop on the use of parallel processors in meteorology), World Scientific

Hellerman S, Rosenstein M (1983) Normal monthly wind stress over the World Ocean with error estimates. J Phys Oceanogr 13:1093–1104

Herman GF, Johnson WT (1980) The effect of extreme sea ice variations on the climatology of the Goddard general circulation model. In: Pritchard ED (ed) Sea ice processes and models. University of Washington, Seattle, pp 207–223

Levitus S (1982) Climatological atlas of the Word Ocean. NOAA Prof Pap 13, CS Government Printing Office, Washington D.C.

Marti O, Madec G, Delecluse P (1992) Comment on "net diffusivity in ocean general circulation models with nonuniform grids" by F. L. Yin and I. Y. Fung. J Geophys Res 97:12763–12766

Murray RJ (1995) Explicit generation of orthogonal grids for ocean models. J Comput Phys (accepted)

Mysak LA, Manak DK, Marsden RF (1990) Sea-ice anomalies observed in the Greenland and Labrador Seas during 1901–1984 and their relation to an interdecadal Arctic climate cycle. Clim Dyn 5:111–133

Reason CJC, Power SB (1994) The influence of the Bering Strait on the circulation in a coarse resolution global ocean model. Clim Dyn 9:363–369

Rudels B (1989) The formation of polar surface water, the ice export and the exchanges through Fram Strait. Prog Oceanogr 22:205–248

Semtner AJ, Chervin RM (1988) A simulation of the global ocean circulation with resolved eddies. J Geophys Res 93:15502–15522

Semtner AJ, Chervin RM (1992) Ocean general circulation from a global eddy-resolving model. J Geophys Res 97:5493–5550

Washington WM, Meehl GA (1986) General circulation model CO_2 sensitivity experiments: snow-sea ice albedo parameterization and globally averaged surface air temperature. Clim Change 8:231–241